

Thermodynamic integration, fermion sign problem, and real-space renormalization

Koka Sathwik^{1†} and Werner Krauth^{1, 2*}

¹ Laboratoire de Physique de l'École normale supérieure, ENS, Université PSL, CNRS, Sorbonne Université, Université Paris-Diderot, Sorbonne Paris Cité, Paris, France

² Rudolf Peierls Centre for Theoretical Physics, Clarendon Laboratory, Oxford OX1 3PU, UK

† koka.sathwik@ens.psl.eu * werner.krauth@ens.fr

Abstract

We reconsider real-space renormalization for the two-dimensional Ising model, following the path traced out by Wilson in Sect. VI of his 1975 Reviews of Modern Physics [1]. In that reference, Wilson considerably extended the Kadanoff decimation procedure towards a possibly rigorous construction of a real-space scale-invariant hamiltonian. Wilson's construction has, to the best of our knowledge, never been fully understood and thus neither reproduced nor generalized. In the present work, we use Monte Carlo sampling in combination with thermodynamic integration in order to retrace Wilson's computation for a real-space renormalization with a number of terms in the hamiltonian. We elaborate on the connection of real-space renormalization with the fermion sign problem and discuss to which extent our Monte Carlo procedure actually implements Wilson's program from half a century ago.

Copyright attribution to authors.

This work is a submission to SciPost Physics.

License information to appear upon publication.

Publication information to appear upon publication.

Received Date

Accepted Date

Published Date

Contents

1	Introduction	2
2	Decimation—real-space renormalization	2
2.1	Wilson patch	3
2.2	Kadanoff's original decimation, flaw	4
2.3	Modified decimation, coupling parameter ρ	4
3	Markov-chain Monte Carlo procedure	5
3.1	Thermodynamic integration	5
3.2	Fermion sign problem	6
3.3	Correlated sampling	8
4	Computational results	8
4.1	Two factor types: integration path, average sign	9
4.2	Two factor types: correlated sampling, fixpoint	9
4.3	Fourteen factor types	11

5	Conclusions	11
A	Perturbative fixpoint for two factor types	12
B	Enumeration of new central spins	13
C	Access to computer programs	13
	References	14

1 Introduction

The renormalization group [1], a cornerstone of theoretical physics, originates in the concept of universality in statistical mechanics. It implements that the physics on large length scales, at a critical point, is described through a few models that differ qualitatively, for example through the symmetries of their hamiltonians. A renormalization procedure computes properties of the system from the constraint of having to arrive at such a distinct model in the limit. A prominent variant of the theory is real-space renormalization. It was pioneered by Kadanoff [2] as a decimation procedure in which half of the spins are eliminated (integrated out), and the remaining ones identified from one iteration of the renormalization procedure to the next one. As analyzed by Wilson, this renormalization consists in computing the partition function at the critical point, where the correlation length becomes infinite, and where spin–spin correlations decay as power laws. At this critical point, the fixpoint hamiltonian of the system is described by universal coupling constants. Despite its conceptual appeal as a direct application of scale invariance, real-space renormalization has mainly been presented in a pedagogical context [3], with only a few quantitative applications [4–9]. Nevertheless, Wilson has shown Ref. [1, Section VI] that real-space renormalization can avoid the collapse of spin–spin correlations by decimating (as before) half of the spins but without identifying the remaining spins over the iterations of the renormalization. This explicitly constructs the scale-invariant hamiltonian and allows for the computation of critical exponents. Wilson’s computation for the Ising model has been notoriously difficult to reproduce [10], and has not been generalized. The present work rephrases Wilson’s computation in the language of modern computational physics and reproduces some of its results by unbiased Monte Carlo sampling methods that involve thermodynamic integration [11] and that treat an emergent fermionic sign problem [12]. This work is self-contained (see Appendix A). Our algorithms merely aim at a proof of concept. They are implemented as Python scripts and are openly available (see Appendix C).

2 Decimation—real-space renormalization

Real-space renormalization consists, in a nutshell, in setting up a very general hamiltonian for the interaction of Ising spins and then in integrating out a certain fraction of the spins and in writing the result as the same hamiltonian. In real space, this hamiltonian must have many more terms beyond the usual nearest-neighbor interaction of the Ising model which, by itself, is not invariant under scale transformations.

We use factors to generalize the pairs of nearest-neighbor spins in the usual Ising model.

Each factor M is defined through a set I_M of site indices on which it couples the spins. The index set I_M implies a certain type T_M (two neighboring sites, two next-nearest neighbors, four sites around a fundamental plaquette, etc.). For clarity and ease of book-keeping, we write each factor as $M := (I_M, T_M)$, although the type is implied by the index set. Index sets I_M and $I_{M'}$ that are related by rotations, reflections and translations satisfy $T_M = T_{M'}$. An interaction K_T is associated with each factor type T , so that the energy of a configuration of spins s_S is:

$$H(s_S) = \sum_{M=(I_M, T_M) \in \mathcal{M}} K_{T_M} \prod_{j \in I_M} s_j. \quad (1)$$

The number of possible factors is huge, potentially as big as the powerset (the set of subsets) of all indices. Ref. [1, Table III] provides 14 dominant factor types $T \in \{1, \dots, 14\}$ (see Fig. 1). We consider two cases, one where the set \mathcal{M} of factors with non-zero weight have $T \in \{1, 2\}$ (nearest and next-nearest neighbors), and the other where all 14 factor types in Fig. 1 are taken into consideration.

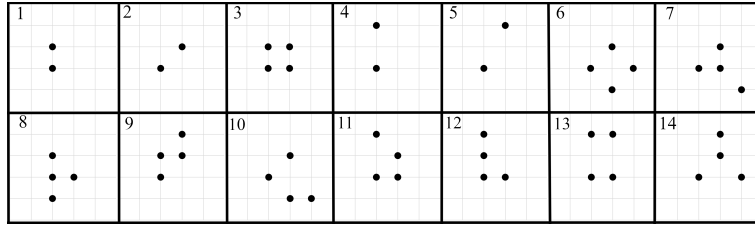


Figure 1: The 14 dominant factor types $T \in \{1, \dots, 14\}$ identified in Ref. [1, Table III]. In the Wilson patch of old sites (set \mathcal{S} of eq. (2)), they appear in 9447 factors. In the patch of new sites (set \mathcal{N} of eq. (4)), they appear in 4795 factors.

2.1 Wilson patch

Figure 2, reproduced from Ref. [1, Fig. 8], defines the *Wilson patch* to which we restrict our attention throughout this work. It consists in a finite two-dimensional square lattice with, at iteration i , a set \mathcal{S} of 221 sites, of which 17 sites are located inside the *old central region* \mathcal{B} , with the rest in the *old periphery* \mathcal{A} . In the next iteration, $i + 1$, a set \mathcal{N} of 121 new sites remains, with 11 in the *new central region* $\mathcal{B} \cap \mathcal{N}$. Our numbering scheme assigns the same indices for \mathcal{S} and for \mathcal{N} :

$$\mathcal{S} = \{1, \dots, 221\} \quad |\mathcal{S}| = 221 \quad \text{old sites,} \quad (2)$$

$$\mathcal{O} = \{12, 13, \dots, 21, \dots\} \quad |\mathcal{O}| = 100 \quad \text{“old-only” sites,} \quad (3)$$

$$\mathcal{N} = \mathcal{S} \setminus \mathcal{O} \quad |\mathcal{N}| = 121 \quad \text{new sites,} \quad (4)$$

$$\mathcal{B} = \{89, 90, \dots, 134\} \quad |\mathcal{B}| = 17 \quad \text{old central sites,} \quad (5)$$

$$\mathcal{A} = \mathcal{S} \setminus \mathcal{B} \quad |\mathcal{A}| = 204 \quad \text{old “peripheral” sites,} \quad (6)$$

$$\mathcal{B} \cap \mathcal{N} = \{89, 90, \dots, 133, 134\}, \quad |\mathcal{B} \cap \mathcal{N}| = 11 \quad \text{new central sites.} \quad (7)$$

Following the notations in Ref. [1], we refer to the “old” spins as “ $s \in \{-1, 1\}$ ” and to the “new” spins as “ $t \in \{-1, 1\}$ ”, writing for example $s_S = \{s_i : i \in \mathcal{S}\}$ for the set of old spins and $t_{\mathcal{N}} = \{t_i : i \in \mathcal{N}\}$ for the set of new spins. Likewise, we write $t_{\mathcal{B} \cap \mathcal{N}} = \{t_i : i \in \mathcal{B} \cap \mathcal{N}\}$ for the new central spins, etc.. The 2^{11} spin configurations in the new central region $\mathcal{B} \cap \mathcal{N}$ are numbered using the Gray code (see Appendix B).

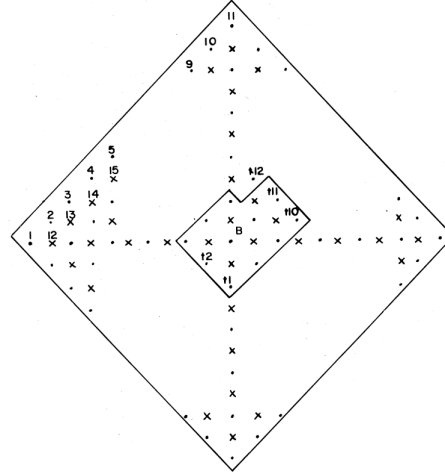


Figure 2: Wilson patch from Ref. [1]. Naively, the old-only spins—the “x” in the picture—are to be decimated (summed over) (see Section 2.2), yielding a partition function and at the same time the Boltzmann weight of the new spins—the “.” in the picture. At the fixpoint, the partition function over the old spins agrees with the Boltzmann weight of the new spins. The naive procedure has a flaw, which was corrected by Kadanoff (see Section 2.3).

2.2 Kadanoff’s original decimation, flaw

Kadanoff’s original decimation consists in integrating out (that is, summing over) the old-only spins $s_{\mathcal{O}}$ for a fixed configuration of new spins:

$$Z(\underbrace{t_{\mathcal{B}\mathcal{N}}|t_{\mathcal{A}\mathcal{N}}}_{\text{fix all new spins } t_{\mathcal{N}}}) = \sum_{s_{\mathcal{O}}|s_{\mathcal{N}}=t_{\mathcal{N}}} \exp[H(s_{\mathcal{S}})]. \quad (8)$$

On the Wilson patch of Fig. 2, the sum on the right-hand side of the above equation involves $|s_{\mathcal{O}}| = 100$ “old-only” spins, and thus runs over 2^{100} terms. All the new spins t are then fixed, so that the above partition function corresponds to a single configuration of t -spins. At the fixpoint, the latter is the exponential of the hamiltonian for the t spins:

$$Z(t_{\mathcal{B}\mathcal{N}}|t_{\mathcal{A}\mathcal{N}}) \stackrel{!}{=} \exp[H(t_{\mathcal{B}\mathcal{N}}|t_{\mathcal{A}\mathcal{N}})]. \quad (9)$$

In Ref. [1], Wilson fixes the outer spins as $t_{\mathcal{A}\mathcal{N}} = \{1, \dots, 1\}$. Varying the 11 new spins $t_{\mathcal{B}\mathcal{N}}$ then leaves 2^{11} equations to be satisfied, which allows one to search for a fixpoint.

The decimation just described has a flaw that arises from the identification of old spins that survive the decimation with the new spins, in other words from the condition $s_{\mathcal{N}} = t_{\mathcal{N}}$ on the right-hand side of eq. (8). The identification impacts the scaling of spin–spin correlation functions at the critical point. Indeed, as first understood by Kadanoff (cited in Ref. [1]), certain lattice points belong to many iterations of the renormalization procedure and under the original decimation, the spins and the spin–spin correlations are identical across iterations. This implies that the spin–spin correlations must be independent of distance and, in fact, zero. At the critical point, where one knows that the decay of correlations is algebraic, this is inconsistent.

2.3 Modified decimation, coupling parameter ρ

To repair the flaw, one considers, following Kadanoff, a decimation procedure that does not identify the surviving old spins with the new spins. The old-only spins are still integrated out.

New and old spins on \mathcal{N} , that is, $s_{\mathcal{N}}$ and $t_{\mathcal{N}}$, are coupled through the following ansatz (see Fig. 3):

$$Z_{\rho}(t_{\mathcal{B}\cap\mathcal{N}}|t_{\mathcal{A}\cap\mathcal{N}}) = \sum_{s_{\mathcal{S}}} \left\{ \exp[H(s_{\mathcal{S}})] \prod_{k \in \mathcal{N}} (1 + \rho t_k s_k) \right\}. \quad (10)$$

Here, the coupling parameter ρ is larger than one. As $t_k, s_k \in \{-1, 1\}$, the final term on the right-hand side of eq. (10) can thus be positive or negative, and Z_{ρ} resembles a fermion partition function.

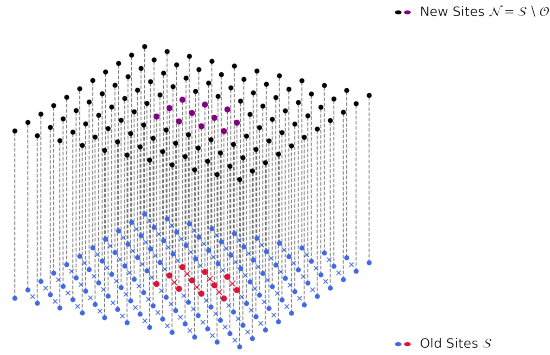


Figure 3: Wilson patch with the modified decimation. All s spins (lower-level crosses and dots) are summed over in order to compute the effective interaction between t spins (upper-level dots). Spins s_k and t_k , for $k \in \mathcal{N}$ (dots on the same sites on both levels) are coupled by $1 + \rho t_k s_k$ (vertical lines), but not identified (see eq. (10)).

3 Markov-chain Monte Carlo procedure

Wilson, in Ref. [1], approximately evaluated Z_{ρ} in eq. (10), using a procedure that was not fully explained. We compute this partition function exactly using Monte Carlo methods. In the present section, we discuss the three main ingredients of this computation. The first is thermodynamic integration (Section 3.1) which allows one to compute a partition function, rather than the expectation of an observable. The second ingredient is the treatment of the fermion sign problem (Section 3.2) that arises from the presence, for $\rho > 1$, of negative contributions to the partition function. On the Wilson patch, the fermion sign problem is not generally severe, and we can evaluate $Z(t_{\mathcal{B}\cap\mathcal{N}}|t_{\mathcal{A}\cap\mathcal{N}})$ because negative and positive contributions do not cancel and the average sign remains non-zero. Finally, we discuss correlated sampling (Section 3.3), which is crucial because we ultimately have to solve a fixpoint equation, in other words a minimization problem. At the minimum, to be determined, we must state that the solution is “better” than at all nearby values in a high-dimensional space. Correlated sampling allows one to make that statement with vanishing statistical errors. We also point out other potential uses of correlated sampling.

3.1 Thermodynamic integration

The fixpoint equation requires the computation of the partition function Z_{ρ} , in other words the computation of a free energy. This requires thermodynamic integration (see [11, Sect. 1.4.2]

for an introduction). In essence, given two unnormalized weight functions π_x and π'_x in a given sample space Ω , neither the partition function $Z = \sum_{x \in \Omega} \pi_x$ nor the partition function $Z' = \sum_{x \in \Omega} \pi'_x$ can be sampled directly without visiting all of Ω . However, the ratio of the two partition functions is given by

$$\frac{Z'}{Z} = \frac{\sum_x \pi'_x}{\sum_x \pi_x} = \frac{\sum_x \pi_x (\pi'_x / \pi_x)}{\sum_x \pi_x} = \left\langle \frac{\pi'_x}{\pi_x} \right\rangle_{\pi}, \quad (11)$$

that is, by an average of the observable π'/π over the distribution π , which can be obtained through Monte-Carlo sampling. In practice, to compute Z'/Z with high precision, the fluctuations of $\pi'(x)/\pi(x)$ and, thus, the difference between π and π' must be small.

In our context, we consider the auxiliary partition function with an additional parameter α allowing for small differences between nearby parameters:

$$Z_{\rho}^{\{\alpha\}}(t_{\mathcal{N}}) = \sum_{s_S} \left\{ \exp[\alpha H(s_S)] \prod_{k \in \mathcal{N}} (1 + \rho t_k s_k) \right\}, \quad 0 \leq \alpha \leq 1. \quad (12)$$

This auxiliary partition function takes on the values

$$Z_{\rho}^{\{\alpha\}}(t_{\mathcal{N}}) = \begin{cases} 2^{|\mathcal{S}|} & \text{for } \alpha = 0 \\ Z_{\rho}(t_{\mathcal{N}}) & \text{for } \alpha = 1 \text{ (see eq. (10)).} \end{cases} \quad (13)$$

The case $\alpha = 0$ corresponds, in a free-energy computation, to the high-temperature or zero-density limit of a physical system, where the free energy is known analytically. The parameter α is thus a fictitious inverse temperature.

To compute Z_{ρ} , we consider a sequence of n values of α : $1 = \alpha_1 > \alpha_2 > \dots > \alpha_n = 0$ and, likewise, a sequence of n values of ρ : $\rho = \rho_1 \simeq \rho_2 \simeq \dots \simeq \rho_n$ and write the telescopic product as

$$Z_{\rho}^{\{\alpha=1\}}(t_{\mathcal{N}}) = \frac{Z_{\rho_1}^{\{\alpha_1\}} Z_{\rho_2}^{\{\alpha_2\}}}{Z_{\rho_2}^{\{\alpha_2\}} Z_{\rho_3}^{\{\alpha_3\}}} \dots \frac{Z_{\rho_{n-1}}^{\{\alpha_{n-1}\}} Z_{\rho_n}^{\{\alpha_n\}}}{Z_{\rho_n}^{\{\alpha_n\}} Z_{\rho_n=0}^{\{\alpha_n\}}}, \quad (14)$$

where, on the right-hand side, we have omitted the dependence on $t_{\mathcal{N}}$. Each of the ratios in this expression can be sampled in principle, but not in practice, because of the presence of positive and negative terms in the partition function.

3.2 Fermion sign problem

For $\rho > 1$, the sum in eq. (12) has positive and negative contributions, and the individual terms can thus not be interpreted as probabilities. Following a classic reference by Blankenbecler et al. [12], we therefore replace the term $\Pi_{\rho} := \prod_{k \in \mathcal{N}} (1 + \rho t_k s_k)$ by its absolute value. Dividing by and multiplying with $|\Pi_{\rho}|$, any of the ratios in eq. (14) can be written as:

$$\frac{Z_{\rho'}^{\{\alpha'\}}(t_{\mathcal{N}})}{Z_{\rho}^{\{\alpha\}}(t_{\mathcal{N}})} = \frac{\sum_{s_S} \exp[\alpha' H(s_S)] |\Pi_{\rho'}| \frac{\Pi_{\rho'}}{|\Pi_{\rho'}|}}{\sum_{s_S} \exp[\alpha H(s_S)] |\Pi_{\rho}| \frac{\Pi_{\rho}}{|\Pi_{\rho}|}}. \quad (15)$$

We finally divide both the numerator and the denominator, by $\sum \exp(\alpha H) |\Pi|$ to arrive at:

$$\frac{Z_{\rho'}^{\{\alpha'\}}(t_{\mathcal{N}})}{Z_{\rho}^{\{\alpha\}}(t_{\mathcal{N}})} = \frac{\langle \exp[(\alpha' - \alpha)H] \Pi_{\rho'} / |\Pi_{\rho}| \rangle_{\alpha, |\rho|}}{\langle \Pi_{\rho} / |\Pi_{\rho}| \rangle_{\alpha, |\rho|}}, \quad (16)$$

where $\langle \dots \rangle_{\alpha, |\rho|}$ refers to expectation values with respect to

$$\pi_{|\rho|}^{\{\alpha\}}(s_S | t_N) = \exp[\alpha H(s_S)] |\Pi_\rho|, \quad (17)$$

which is an unnormalized probability distribution in the sample space Ω of old-site spin configurations of size $|\Omega| = 2^{2N}$. In the denominator of eq. (16), we identify

$$\langle \Pi_\rho / |\Pi_\rho| \rangle_{\alpha, |\rho|} = \langle \text{sign}(\Pi_\rho) \rangle_{\alpha, |\rho|}, \quad (18)$$

in other words the average sign of the partition function. In our application, this average sign usually differs markedly from zero, and the relevant observable averages can still be computed. The sign problem is well known from many low-temperature fermionic Monte Carlo simulations. For $\alpha = 0$, the partition function does not depend on the spins s_O , and the average sign is given by

$$\langle \text{sign} \Pi_\rho \rangle_{|\rho|} = \frac{\sum_{s_S} \prod_{k \in \mathcal{N}} |(1 + \rho s_k)| \text{sign} \Pi_\rho}{\sum_{s_S} \prod_{k \in \mathcal{N}} |(1 + \rho s_k)|} = \frac{\prod_{k \in \mathcal{N}} \sum_{s_k} (1 + \rho s_k)}{\prod_{k \in \mathcal{N}} \sum_{s_k} |(1 + \rho s_k)|} = \frac{2^{|\mathcal{N}|}}{(2\rho)^{|\mathcal{N}|}} = \rho^{-12N}, \quad (19)$$

a formula that will provides a useful check of our simulation results for small values of α . We will later discuss that a *severe* sign problem appears for some configurations $t_{B \cap \mathcal{N}}$ at large ρ , but they can be excluded from our procedure.

```

procedure alpha-rho-Metropolis
input  $s_S, H, \Pi_\rho, \Pi_{\rho'}$  (see eq. (16))
 $i \leftarrow \text{choice}(\{s_S\})$ 
 $\Delta H \leftarrow -2 \sum_{M \in \mathcal{M}: i \in I_M} K_{T_M} \prod_{j \in I_M} s_j$ 
 $\Gamma_\rho \leftarrow 1; \Gamma_{\rho'} \leftarrow 1$ 
if  $i \in \mathcal{N}$ :
   $\left\{ \begin{array}{l} \Gamma_\rho \leftarrow (1 - \rho t_i s_i) / (1 + \rho t_i s_i) \\ \Gamma_{\rho'} \leftarrow (1 - \rho' t_i s_i) / (1 + \rho' t_i s_i) \end{array} \right.$ 
 $\Upsilon \leftarrow \text{ran}(0, 1)$ 
if  $\Upsilon < |\Gamma_\rho| \exp(\alpha \Delta H)$ :
   $\left\{ \begin{array}{l} s_i \leftarrow -s_i \\ H \leftarrow H + \Delta H \\ \Pi_\rho \leftarrow \Gamma_\rho \Pi_\rho \\ \Pi_{\rho'} \leftarrow \Gamma_{\rho'} \Pi_{\rho'} \end{array} \right.$ 
output  $s_S, H, \Pi_\rho, \Pi_{\rho'}$ 

```

Algorithm 1: alpha-rho-Metropolis. One iteration of the single-spin-flip Metropolis algorithm for sampling spin configurations s_S with the distribution $\pi_{|\rho|}^{\{\alpha\}}(s_S | t_N)$. The algorithm provides for the computation of the ratio of partition functions in eq. (16) and of the average sign (see Appendix C for a Python implementation).

Algorithm 1 (alpha-rho-Metropolis) samples spin configurations s_S from the (α, ρ) -dependent Boltzmann distribution of eq. (17). It requires, initially (and optionally), the evaluation of H through eq. (1), but then updates H through increments ΔH . It computes $Z_\rho^{\{\alpha=1\}}(t_N)$ without systematic error. The ratio computations of eq. (16) have a favorable propagation of the error which, at $\alpha' = \alpha$ and $\rho' = \rho$, vanishes identically and then grows as the two sets of parameters drift apart. The downside of Alg. 1 (alpha-rho-Metropolis) is the

absence of correlation between $Z_\rho^{\{\alpha=1\}}(t_{\mathcal{N}})$ and $Z_\rho^{\{\alpha=1\}}(t'_{\mathcal{N}})$ for $t_{\mathcal{N}} \neq t'_{\mathcal{N}}$, in other words the statistical independence of calculations of different new \mathbf{B} spins (see Section 3.3 for possible correlated samplings for $t_{\mathcal{N}} \neq t'_{\mathcal{N}}$).

3.3 Correlated sampling

To locate the fixpoint to high precision, we must compute the change of the partition function $Z_\rho(t_{\mathcal{B}\cap\mathcal{N}}|t_{\mathcal{A}\cap\mathcal{N}})$ and of other functions with small variations of the interactions \mathbf{K}_T , that is, of the hamiltonian \mathbf{H} to a neighboring one \mathbf{H}' . For the computation of gradients, the variations are infinitesimal. Naively, under the rules of Gaussian error propagation, the error bars in $Z_\rho^{\{\mathbf{H}\}}$ and $Z_\rho^{\{\mathbf{H}'\}}$ add up when determining their differences, so that the relative error explodes for $\mathbf{H} \simeq \mathbf{H}'$. Correlated sampling overcomes this problem to a large part. For the computation of the ratio of the two partition functions, it follows from an extension of eq. (16) with the replacements $\alpha\mathbf{H} \rightarrow \mathbf{H}$ and $\alpha'\mathbf{H} \rightarrow \mathbf{H}'$ that:

$$\frac{Z_\rho^{\{\mathbf{H}'\}}(t_{\mathcal{N}})}{Z_\rho^{\{\mathbf{H}\}}(t_{\mathcal{N}})} = \frac{\langle \exp(\mathbf{H}' - \mathbf{H}) \Pi_\rho / |\Pi_\rho| \rangle_{\alpha=1, |\rho|}}{\langle \Pi_\rho / |\Pi_\rho| \rangle_{\alpha=1, |\rho|}}. \quad (20)$$

The quantities relating to \mathbf{H}' or to \mathbf{H} are now evaluated for identical samples \mathbf{s}_S . The statistical error vanishes if \mathbf{H}' and \mathbf{H} are the same, and it remains manageable as long as \mathbf{H}' and \mathbf{H} have similar weights for the same samples \mathbf{s}_S . This eliminates the Gaussian error propagation (see Section 4.2 for a practical application in our context).

Correlated sampling can be extended in many ways, most trivially to small variations in ρ . We have not tested the correlated sampling of partition functions for two different configurations $t_{\mathcal{B}\cap\mathcal{N}}$, that is, of the ratio

$$\frac{Z_\rho^{\{\mathbf{H}\}}(t'_{\mathcal{N}})}{Z_\rho^{\{\mathbf{H}\}}(t_{\mathcal{N}})} = \frac{\langle \exp(\mathbf{H}(t'_{\mathcal{N}}) - \mathbf{H}(t_{\mathcal{N}})) \Pi_\rho / |\Pi_\rho| \rangle_{\alpha, t_{\mathcal{N}}, |\rho|}}{\langle \Pi_\rho / |\Pi_\rho| \rangle_{\alpha, t_{\mathcal{N}}, |\rho|}}. \quad (21)$$

This procedure would correlate the samples and greatly reduce the relative error of the computation for different values of $t_{\mathcal{B}\cap\mathcal{N}}$, what eq. (20) does not achieve. We expect pairs of configurations $t_{\mathcal{B}\cap\mathcal{N}}$ which differ in one or two spins to be open to correlated sampling. Propagation as in Section 3.3 would then allow to correlate all partition functions $Z_\rho^{\{\mathbf{H}\}}$ with negligible statistical errors, and therefore greatly improve the calculation of the variation ratio of Section 4. In this scheme, the integration over different configurations $t_{\mathcal{B}\cap\mathcal{N}}$ replaces, up to an irrelevant multiplicative constant, the thermodynamic integration over the fictitious inverse temperature α .

4 Computational results

We have implemented Alg. 1 (alpha-rho-Metropolis), as a proof of concept, in an elementary Python script that is publicly accessible (see Appendix C). It reads in the \mathcal{S} , \mathcal{O} , and \mathcal{B} indices, as well as the factors. Following Ref. [1], all new spins $t_{\mathcal{A}\cap\mathcal{N}}$ in the periphery are set to +1. We thus compute, using Alg. 1 (alpha-rho-Metropolis), the ratio

$$\Theta(t_{\mathcal{B}\cap\mathcal{N}}|t_{\mathcal{A}\cap\mathcal{N}}) = \frac{Z_\rho^{\{\alpha=1\}}(t_{\mathcal{B}\cap\mathcal{N}}|t_{\mathcal{A}\cap\mathcal{N}} = \{1, \dots, 1\})}{\exp[H(t_{\mathcal{B}\cap\mathcal{N}}|t_{\mathcal{A}\cap\mathcal{N}} = \{1, \dots, 1\})]} \stackrel{!}{=} \text{const}, \quad (22)$$

which should be constant at a fixpoint. For our numerically rigorous integration procedure, we do not expect an exact fixpoint to exist for a small number of factor types. Nevertheless,

a finite- K fixpoint can be defined as the choice of interactions K_T minimizing the “variation ratio”

$$\Psi(\{K_T\}|t_{\mathcal{A}\cap\mathcal{N}}) = \frac{\sqrt{\langle\Theta(t_{\mathcal{B}\cap\mathcal{N}}|t_{\mathcal{A}\cap\mathcal{N}})^2\rangle_{t_{\mathcal{B}\cap\mathcal{N}}} - [\langle\Theta(t_{\mathcal{B}\cap\mathcal{N}}|t_{\mathcal{A}\cap\mathcal{N}})\rangle_{t_{\mathcal{B}\cap\mathcal{N}}}]^2}}{\sqrt{\langle\Theta(t_{\mathcal{B}\cap\mathcal{N}}|t_{\mathcal{A}\cap\mathcal{N}})^2\rangle_{t_{\mathcal{B}\cap\mathcal{N}}}}} \quad (23)$$

The variation ratio $\Psi(\{K_T\}|t_{\mathcal{A}\cap\mathcal{N}})$ is zero when the fixpoint condition of eq. (22) is satisfied for the same constant for all inner spins $t_{\mathcal{B}\cap\mathcal{N}}$, in other words, at a fixpoint. We can practically compute Ψ by averaging over the 2^{11} configurations of t -spins in $\mathcal{B}\cap\mathcal{N}$, or a sufficiently large subset thereof.

4.1 Two factor types: integration path, average sign

Algorithm alpha-rho-Metropolis is tested for two factor types ($T = 1$ and $T = 2$ in Fig. 1) with non-vanishing interactions K_1 and K_2 that, for coherence with Wilson’s notations, we call K and L . We then deal with **800** factors for the old spins $s_i : i \in S$ and **420** factors for the new ones. For this two-factor-type model, Wilson has obtained the non-trivial fixpoint in second-order perturbation theory as

$$K^* = (2\rho^2 + \rho^4)^{-1} \quad (24)$$

$$L^* = \rho^2(2\rho^2 + \rho^4)^{-2} \quad (25)$$

(see Appendix A for a self-contained derivation). For a coupling parameter $\rho = 1.04$, the perturbation-theory fixpoint is at $K^* = 0.3, L^* = 0.10736$. For these interactions, we have studied in detail the average “fermion” sign of eq. (18) as a function of α and ρ . For ρ somewhat larger than **1.006**, the average sign approaches zero and the sign problem thus becomes severe for $\alpha \rightarrow 0$ (see eq. (19)). The integration path (the chain of pairs (α, ρ) and (α', ρ') leading towards $\alpha = 0$) thus has to move to smaller ρ , as shown in Fig. 4a for a specific choice of $t_{\mathcal{B}\cap\mathcal{N}}$ spins. For locating the fixpoint, we need to compute the partition function for a number of different $t_{\mathcal{B}\cap\mathcal{N}}$ spins. We have monitored the sign problem at $\alpha = 1$ for the 2^{11} different $t_{\mathcal{B}\cap\mathcal{N}}$ spin configurations and found it to be manageable for almost all choices at $\rho = 1.05$, and for all choices of $t_{\mathcal{B}\cap\mathcal{N}}$ for smaller ρ (see Fig. 4b). A Python script for this computation is available in Appendix C.

4.2 Two factor types: correlated sampling, fixpoint

To illustrate the force of correlated sampling, we consider, in the two-factor-type model, the calculation of partition functions $Z_\rho^{\{\alpha=1\}}$ for the interactions $(K, L) = (0.301, 0.10736)$ and the nearby $(K, L) = (0.3, 0.10736)$. Independent computations with $\sim 2 \times 10^8$ samples distributed over the thermodynamic integration from $\alpha = 1$ to $\alpha = 0$ with **10** intermediate values of ρ and α yield an estimate of the ratio of these partition functions as 1.388 ± 0.04 . Correlated sampling (using eq. (20)) requires no thermodynamic integration, and 1×10^7 samples yield the ratio of these partition functions to 1.3994 ± 0.0001 . It thus gains several orders of magnitude in precision (see Appendix C for example programs retracing this computation).

For our proof-of-concept computation, we have not implemented our correlated-sampling ideas but simply computed the variation ratio $\Psi[(K, L)|t_{\mathcal{B}\cap\mathcal{N}} = \{1, \dots, 1\}]$ from independently computed partition functions (using thermodynamic integration over **10** intermediate values of ρ and α) for a grid of values of K and L . In Fig. 5, we plot the variation ratio Ψ of eq. (23) for $\rho = 1.04$. The variation ratio is smallest for $(K, L) \simeq (0.31, 0.11)$, in good agreement with perturbation theory. To simplify the calculation, and given the small number of interactions K_T to be fitted, Ψ was computed from six of the $t_{\mathcal{B}\cap\mathcal{N}}$ configurations encoded in Table 1 rather than for all **2048**.

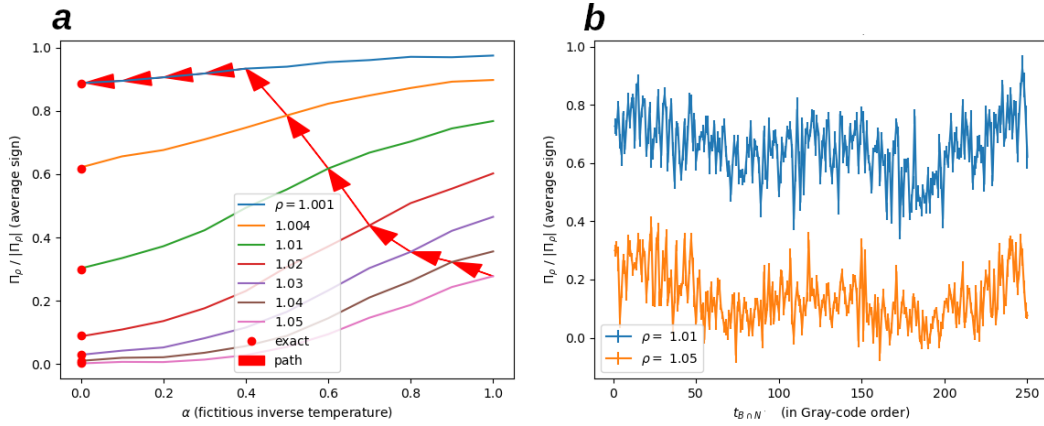


Figure 4: Average sign of Alg. 1 (alpha-rho-Metropolis) for the two-factor-type model with interactions $(K, L) = (0.3, 0.10736)$. (a): Average sign and thermodynamic integration path ($t_{B \cap N} = 2$, $t_{A \cap N} = \{1, \dots, 1\}$) connecting $(\alpha, \rho) = (1, 1.05)$ to the known partition function at $(\alpha, \rho) = (0, 1.001)$, with exact values (red dots) from eq. (19). (b): Average sign at $\alpha = 1$ for the spin configurations $t_{B \cap N} = \{1, \dots, 250\}$, for two different coupling parameters ρ .

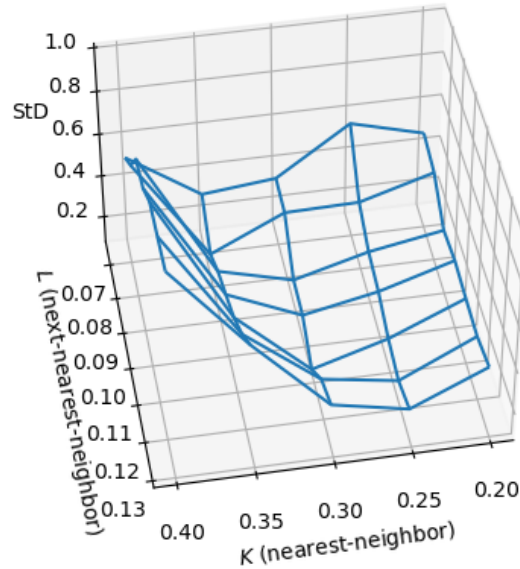


Figure 5: Plot of the variation ratio $\Psi(K, L|\{1, \dots, 1\})$ for the two-factor-field model on a grid of interactions (K, L) for correlation parameter $\rho = 1.04$. The variations are smallest for $(K, L) \simeq (0.31, 0.11)$, in good agreement with second-order perturbation theory.

4.3 Fourteen factor types

For the fourteen factor types in Fig. 1, we have **9447** factors for the old spins and **4795** factors for the new spins. For this problem, we have restricted ourselves to the computation of the average sign for the **14** values of K_T given in [1, Table III] (see Fig. 6), which appears roughly as for the two-factor-field model in Fig. 4. Globally, we conclude that the sign problem remains under control.

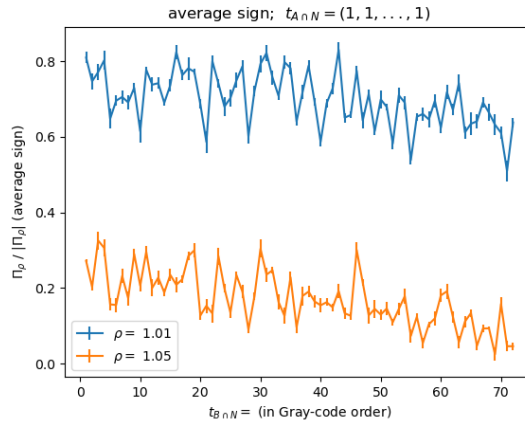


Figure 6: Average sign of Alg. 1 (alpha-rho-Metropolis) for $t_{B \cap N} \in \{1, \dots, 72\}$ (see Appendix B for the enumeration), in the fourteen-factor-type model with interactions K_T as in [1, Table III]

5 Conclusions

In this work we have retraced, on the level of a proof of concept, the classic real-space-renormalization computation by Wilson [1], using state-of-the-art Monte Carlo techniques [11]. Our computations can be generalized in many ways, and our publicly accessible Python scripts (see Appendix C) can be extended in directions that we have indicated. They can be rendered many orders of magnitude more precise, through better codes, more adapted computer languages, but mostly through the systematic use of correlated sampling.

Kadanoff and Wilson, half a century ago, modified the original decimation procedure at the core of real-space renormalization in order to allow for non-trivial algebraic scaling of spin-spin correlation functions. In our computational framework, this brings in aspects of fermionic Monte Carlo and of its notorious sign problem [12] which, as we have shown here, can be handled with relative ease. It is unclear to us whether the modified decimation procedure is itself free of contradictions, and if so, whether it is unique and can be generalized beyond the two-dimensional Ising universality class. Our numerical routine for computing the fixpoint uses key Monte Carlo techniques (thermodynamic integration, fermion-sign problem, correlated sampling). Much understanding will have to be built up, though. We have noticed, for example, that the sign problem is more severe for spins $t_{A \cap N}$ differing from Wilson's choice $t_{A \cap N} = \{1, \dots, 1\}$. The significance of the effectively fermionic partition function within classical statistical mechanics needs to be better understood, just as the very definition of a fixpoint as a minimal-variance point for a finite number of factor types which we expect to converge towards a *bona fide* fixpoint in the limit of infinite factor types.

Acknowledgements

We are grateful to Slava Rychkov for support and helpful discussions.

Funding information W. K. acknowledges generous support by the Leverhulme Trust.

A Perturbative fixpoint for two factor types

In this appendix, we derive Wilson’s fixpoint equations in second-order perturbation theory for the two-factor-type model. We consider a sufficiently large lattice to accommodate all hopping terms to second order (see Fig. 7a).

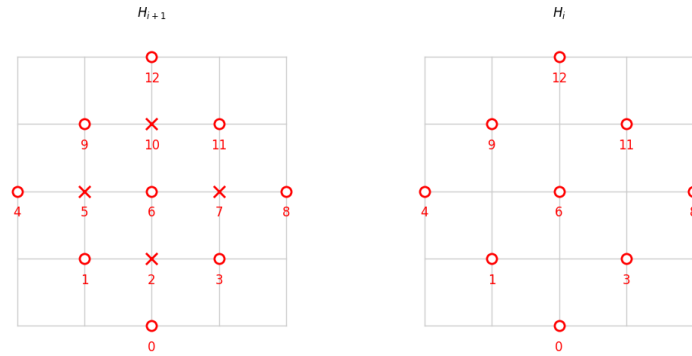


Figure 7: Kadanoff decimation for the two-dimensional Ising model with K and L interactions on a small lattice.

In Kadanoff’s original decimation (see Section 2.2), on this lattice, we integrate out the “only old” spins s_2, s_5, s_7, s_{10} , in order to arrive at the renormalized H_{i+1} on the lattice of new spins Fig. 7b. We have

$$\exp H_{i+1} = \sum_{s_2=\pm 1, s_5, s_7, s_{10}=\pm 1} \exp(K_i s_1 s_2 + K_i s_2 s_3 + \cdots + L_i s_0 s_1 + L_i s_2 s_7 + \cdots + L_i s_{11} s_{12}). \quad (\text{A.1})$$

In eq. (A.1), terms in K_i have one old spin and one new spin, while the terms in L_i have either two old spins or two new spins. We expand the exponential to second order, and keep only terms quadratic in K_i or else linear in L_i . This gives

$$\exp(H_{i+1}) = \sum_{s_2, s_5, s_7, s_{10}} \left[1 + (K_i s_1 s_2 + K_i s_2 s_3 + \cdots + L_i s_0 s_1 + L_i s_2 s_7 + \cdots + L_i s_{11} s_{12}) + \frac{1}{2} (K_i s_1 s_2 + K_i s_2 s_3 + \cdots +)^2 \right]. \quad (\text{A.2})$$

The constant term 1 sums up to $2^4 = 16$. The linear terms in K_i sum to zero. The linear terms in L_i sum to zero if they connect old spins, and they sum up to 16 if they connect new spins. Non-vanishing quadratic terms are of two types. Those connecting a chain of spins are as

$$\frac{1}{2} K_i^2 (s_6 s_7 s_7 s_{11} + s_6 s_{10} s_{10} s_{11}), \quad (\text{A.3})$$

but each term $s_6 s_7 s_7 s_{11}$ appears twice, once with the $s_6 s_7$ in the first of the two braces $(\dots)(\dots)$, and once in the second. The terms coupling s_6 to s_{11} sum up to $16 \times \frac{1}{2} \times 2 \times 2 = 16 \times 2$.

Quadratic terms, such as $\frac{1}{2}K_i^2(\mathbf{s}_0\mathbf{s}_2)^2$, that go from one spin and back, sum up to $16 \times \frac{1}{2} \times 16K_i^2$, as there are 16 edges on this lattice, and in addition 16 spin configurations to be summed over. This yields:

$$\exp(H_{i+1}) = 16 \left[1 + \dots (2K_i^2 + L_i) s_6 s_{11} + \dots + K_i^2 s_6 s_{12} + \dots + 8K_i^2 \right]. \quad (\text{A.4})$$

After re-exponentiation, the s_6, s_{11} interaction corresponds to K_{i+1} and the $s_6 s_{12}$ interaction to L_{i+1} , reproducing Wilsons eqs. (VI.18) and (VI.19). The results would be identical for any larger lattice, as we made at most two hops.

In the modified decimation (see Section 2.3), all spins $\{\mathbf{s}_0 \rightarrow \mathbf{s}_{12}\}$ are summed over in $\exp(H_i)$, and the coupling with the spins t of the hamiltonian H_{i+1} is expressed through ρ . This gives

$$\exp(H_{i+1}) = \sum_{s_0, \dots, s_{12}} \exp(K_i s_0 s_2 + \dots + L_i s_2 s_7 + \dots) \prod_{k=0,1,3,4,6,8,9,11,12} \frac{1 + \rho t_k s_k}{2}. \quad (\text{A.5})$$

We expand the exponential to second order. The constant term gives $2^{13}/2^9 = 2^4$, because in the product term of eq. (A.5), only the $\frac{1}{2}$ terms survive. To linear order, all the K_i terms disappear, because of the presence of an isolated old spin. There are linear L terms, such as

$$L s_6 s_{11} (1 + \rho t_6 s_6) (1 + \rho t_{11} s_{11}) = L t_6 t_{11} \rho^2, \quad (\text{A.6})$$

again multiplied by a factor 16. To second order from 6 to 11, we have a term

$$\sum_{s_0, \dots, s_{12}} \frac{1}{2^9} \frac{1}{2} K_i^2 (s_6 s_7 s_7 s_{11} + s_7 s_{11} s_6 s_7 s_6 s_{10} s_{10} s_{11} + s_{10} s_{11} s_6 s_{10}) s_6 s_{11} \rho^2 t_6 t_{11} = 16 \times 2 K_i^2 \rho^2 t_6 t_{11}, \quad (\text{A.7})$$

whereas the term coupling t_6 and t_{12} is half this one. This yields:

$$\exp(H_{i+1}) = 16 \left[1 + \dots (2K_i^2 + L_i) \rho^2 t_6 t_{11} + \dots + K_i^2 \rho^2 t_6 t_{12} + \dots \right]. \quad (\text{A.8})$$

After re-exponentiation, the t_6, t_{11} interaction corresponds to K_{i+1} and the $t_6 t_{12}$ interaction to L_{i+1} , reproducing Wilsons eqs. (VI.45) and (VI.46), which correspond to our eqs (24) and (25).

B Enumeration of new central spins

Configurations of the 11 new spins $t_{B \cap V}$ in the central regions are required for the study of the sign problem (the computation of the average sign) and for the minimization procedure. For concreteness, we enumerate them using the Gray code (see Table 1). The corresponding Python script is available in our open-source repository (see Appendix C).

C Access to computer programs

This work is accompanied by the MCRRealSpace software package, which is published as an open-source project under the GNU GPLv3 license. MCRRealSpace is available on GitHub as a part of the JeLLyFysh organization. The package contains Python scripts for the algorithms discussed in this work, as well as the data files encoding the Wilson patch, including the factors. The url of the repository is <https://github.com/jellyfysh/MCRealSpace.git>.

number	$t_{89}, t_{90}, \dots, t_{133}, t_{134}$
1	-----
2	-----+
3	-----++
4	-----+-
..	...
820	-+-+--+--+--
..	...
1366	+++++
..	...
1639	+--+--+--+--+
..	...
2048	+-----

Table 1: Numbering scheme for the new spins $t_{B \cap \mathcal{N}}$ in the central region, following the Gray code. The first column of this table corresponds to the x -axis in Fig. 4b (see Appendix C for a Python script).

References

- [1] K. G. Wilson, *The renormalization group: Critical phenomena and the Kondo problem*, Rev. Mod. Phys. **47**, 773 (1975), doi:[10.1103/RevModPhys.47.773](https://doi.org/10.1103/RevModPhys.47.773).
- [2] L. P. Kadanoff, *Variational Principles and Approximate Renormalization Group Calculations*, Phys. Rev. Lett. **34**(16), 1005–1008 (1975), doi:[10.1103/physrevlett.34.1005](https://doi.org/10.1103/physrevlett.34.1005).
- [3] H. J. Maris and L. P. Kadanoff, *Teaching the renormalization group*, Am. J. Phys. **46**(6), 652–657 (1978), doi:[10.1119/1.11224](https://doi.org/10.1119/1.11224).
- [4] T. L. Bell and K. G. Wilson, *Finite-lattice approximations to renormalization groups*, Phys. Rev. B **11**, 3431 (1975), doi:[10.1103/PhysRevB.11.3431](https://doi.org/10.1103/PhysRevB.11.3431).
- [5] R. B. Griffiths and P. A. Pearce, *Position-Space Renormalization-Group Transformations: Some Proofs and Some Problems*, Phys. Rev. Lett. **41**(14), 917–920 (1978), doi:[10.1103/physrevlett.41.917](https://doi.org/10.1103/physrevlett.41.917).
- [6] T. Kennedy, *Some rigorous results on majority rule renormalization group transformations near the critical point*, J. Stat. Phys. **72**(1–2), 15–37 (1993), doi:[10.1007/bf01048038](https://doi.org/10.1007/bf01048038).
- [7] T. Kennedy, *Renormalization Group Maps for Ising Models in Lattice-Gas Variables*, J. Stat. Phys. **140**(3), 409–426 (2010), doi:[10.1007/s10955-010-0002-0](https://doi.org/10.1007/s10955-010-0002-0).
- [8] A. C. D. van Enter, R. Fernández and A. D. Sokal, *Regularity properties and pathologies of position-space renormalization-group transformations: Scope and limitations of Gibbsian theory*, J. Stat. Phys. **72**(5–6), 879–1167 (1993), doi:[10.1007/bf01048183](https://doi.org/10.1007/bf01048183).
- [9] K. Haller and T. Kennedy, *Absence of renormalization group pathologies near the critical temperature. Two examples*, J. Stat. Phys. **85**(5–6), 607–637 (1996), doi:[10.1007/bf02199358](https://doi.org/10.1007/bf02199358).
- [10] S. Rychkov, *private communication* (2023).
- [11] W. Krauth, *Statistical Mechanics: Algorithms and Computations*, Oxford University Press (2006).

- [12] R. Blankenbecler, D. J. Scalapino and R. L. Sugar, *Monte Carlo calculations of coupled boson-fermion systems. I*, Phys. Rev. D **24**, 2278 (1981), doi:[10.1103/PhysRevD.24.2278](https://doi.org/10.1103/PhysRevD.24.2278).